ACS APPLIED MATERIALS & INTERFACES

Research Article

www.acsami.org

Single-Step Direct Fabrication of Pillar-on-Pore Hybrid Nanostructures in Anodizing Aluminum for Superior Superhydrophobic Efficiency

Chanyoung Jeong and Chang-Hwan Choi*

Department of Mechanical Engineering, Stevens Institute of Technology, Castle Point on Hudson, Hoboken, New Jersey 07030, United States

ABSTRACT: Conventional electrochemical anodizing processes of metals such as aluminum typically produce planar and homogeneous nanopore structures. If hydrophobically treated, such 2D planar and interconnected pore structures typically result in lower contact angle and larger contact angle hysteresis than 3D disconnected pillar structures and, hence, exhibit inferior superhydrophobic efficiency. In this study, we demonstrate for the first time that the anodizing parameters can be engineered to design novel pillar-on-pore (POP) hybrid nanostructures directly in a simple one-step fabrication process so that superior surface superhydrophobicity can also be realized effectively from the electrochemical anodization process. On the basis of the characteristic of forming a self-ordered porous morphology in a hexagonal array, the modulation of anodizing voltage and duration enabled the formulation of the hybrid-type nanostructures having controlled pillar morphology on top of a porous layer in both mild and hard anodization modes. The hybrid nanostructures of the anodized metal oxide layer initially enhanced the surface hydrophilicity significantly (i.e., superhydrophilic). However, after a hydrophobic monolayer coating, such hybrid nanostructures then showed superior superhydrophobic nonwetting properties not attainable by the plain nanoporous surfaces produced by conventional anodization conditions. The well-regulated anodization process suggests that electrochemical anodizing can expand its usefulness and efficacy to render various metallic substrates with great superhydrophilicity or -hydrophobicity by directly realizing pillar-like structures on top of a self-ordered nanoporous array through a simple one-step fabrication procedure.

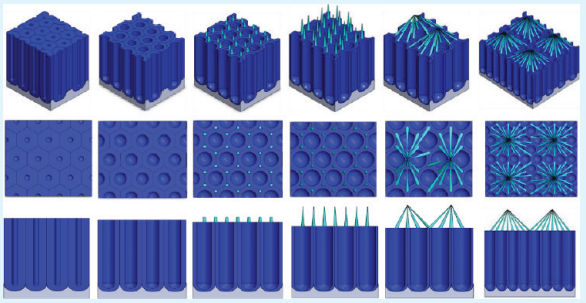

KEYWORDS: *aluminum, anodization, hybrid nanostructure, superhydrophilic, superhydrophobic*

1. INTRODUCTION

Micro- or nanotextured surfaces of low surface energy (e.g., hydrophobic) can create a composite interface with liquid by entraining air between the surface structures due to surface tension effects, resulting in superior nonwetting (i.e., superhydrophobic) properties.[1−3] The superhydrophobic surfaces have recently received great attention due to their highly nonwetting and nonadhesive properties for multifunctional applications such as self-cleaning,[4] low hydrodynamic friction,[5,6] anticorrosion,[7] anti-icing,[8,9] and templates for directed self-assembly of nanomaterials.[10] In the past decade, numerous micro- and nanofabrication techniques have been explored to design and create effective superhydrophobic surfaces.[11−14] However, each method so far developed still requires significant advancement and innovation of the fabrication techniques for real and practical applications of engineered superhydrophobic surfaces. For example, lithographic techniques are excellent for defining precise and well-ordered micro- and nanopatterns. However, they work primarily with only planar substrates at no greater than wafer scale, requiring complicated process steps and expensive equipment. Granular or fibrous coating methods using spraying, sol−gel wet chemistry, or electrospinning are affordable, scalable, and easily applicable to most types of substrates with good remediability. However, the structural patterns and dimensions produced by these methods are randomly distributed and oriented with a lack of regularity. The additive coating methods also have adhesion issues such as delamination and peel-off. In comparison, electrochemical etching techniques such as anodization are considered one of the most promising methods to generate self-ordered nanostructures over large surface areas (even on nonplanar geometries). This is especially the case for metallic substrates important to many civil and military applications, wherein a simple electrolytic passivation process is employed for growing a natural oxide layer. It does not require complex or expensive fabrication facilities and equipment for manufacturing. Anodic films are generally much stronger and more adherent than most types of paint and metal plating. This makes them less likely to crack and peel from aging and wear. However, it should be noted that the electrochemical anodizing process normally forms only 2D homogeneous hexagonal porous structures,

Received: October 31, 2011
Accepted: December 27, 2011
Published: December 27, 2011

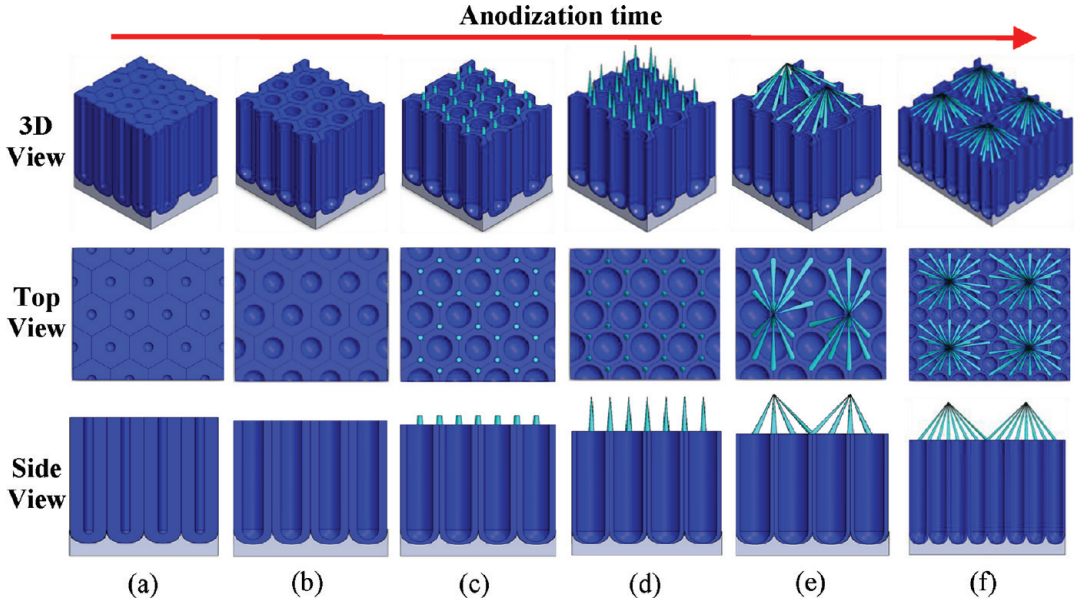

Figure 1. Schematics of the emergence of pillar-on-pore (POP) hybrid nanostructures with the evolution of anodization processes: (a) planar pore (PP) nanostructures; (b) pore-widened PP nanostructures; (c) single pillar-on-pore (S-POP) nanostructures; (d) S-POP nanostructures of high-aspect-ratio sharpened tips; (e) bundled pillar-on-pore (B-POP) nanostructures; (f) B-POP nanostructures of an increased bundle size. The first row represents three-dimensional (3-D) views of the nanostructures, while the second and the third rows represent the top and the cross-sectional views, respectively.

which is not desirable from the perspective of superhydrophobic efficiency.

Typically superhydrophobic nonwetting efficiency is characterized by its high contact angle (e.g., greater than 150°) and low contact angle hysteresis (difference between advancing and receding contact angles) of a sessile droplet measured in both static and dynamics conditions on the surface. Most surface patterns developed and studied for superhydrophobicity have been monolithic, being of either pillar or porous type. The significant difference between pillar and porous structures is that the liquid contact line on the solid surface is discontinuous in pillar-type structures but continuous in pore-type structures.[15] Compared to the continuously interconnected porous patterns, the discontinuous pillar structures generally exhibit superior superhydrophobic efficiency (i.e., a higher contact angle and a lower contact angle hysteresis) because they allow less solid fraction and contact-line boundary to liquid droplets.[16] However, pillar-like discontinuous structures have poor dewetting stability. For example, when the nonwetting state collapses and homogeneous wetting occurs due to the depletion of surface air by various thermodynamic and hydrodynamic effects, the wetting transition in the case of pillar patterns is energetically more favorable than pore patterns so that it propagates and spreads out easily due to the instability.[17] In contrast, porous structures can provide better dewetting stability since the entrapped air layers are isolated within the individual pore structures so that the wetting will be confined within a single individual pore.[15,18] Thus, it is desirable to design and develop novel surface structures that can provide the combined features and merits of both types of structures for superior superhydrophobic efficiency and dewetting stability.

In this paper, we demonstrate that the electrochemical anodization process can be engineered to design and fabricate such combined structures, so-called "pillar-on-pore" hybrid nanostructures, by modulating the anodizing parameters efficiently, so that they can provide superior superhydrophobic efficiency like pillar structures (i.e., high contact angle and low contact angle hysteresis) while retaining good dewetting stability inherent to pore structures. The effects of the nanopillar morphology hybridized on top of the nanoporous layer will also be verified and discussed in regard to superhydrophobic efficiency.

2. FABRICATION SCHEME

Anodization techniques have been widely used in making porous nanostructures on metallic substrates such as aluminum because of their efficient capability of self-ordered nanoscale pore arrangement and the convenient controllability of the pore parameters (e.g., pore size, interpore distance, and the growth rate of an oxide layer) by modulating the anodizing conditions such as voltage, time, and temperature.[19−22] For example, compared to archetypal mild anodization (MA) processes,[23−26] hard anodization (HA) processes use relatively high anodizing voltages to take advantage of an enhanced growth rate of a porous oxide layer with improved ordering of the nanopores.[27] The high voltage is also likely to result in much larger pore sizes than those attainable in MA processes, thereby often giving rise to irregular surface roughness such as protruding tips.[28−30] While such irregularity is not desirable to obtain highly ordered porous structures for typical applications,[31] the new fabrication scheme proposed in this study is to engineer such effects to design and create unique "pillar-on-pore" (POP) hybrid nanostructures for superior superhydrophobic surfaces by modulating the anodization conditions properly.

Figure 1 represents the design and fabrication scheme for the POP hybrid nanostructures using an electrochemical anodizing method with aluminum substrates. Furthermore, Figure 2 schematically illustrates the basic mechanism of the formation of pillar nanostructures directly on a pore layer. If an anodizing voltage is well controlled in anodization processes, the sidewalls of pore structures on a top layer get etched and thinner while a

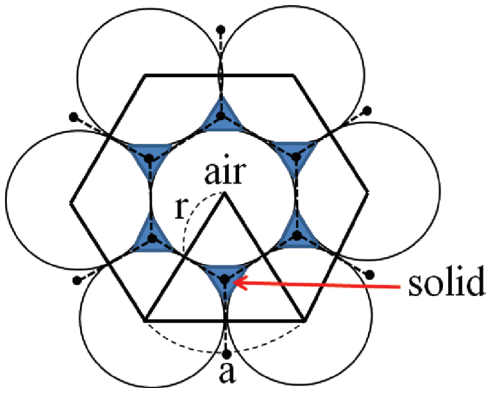

Figure 2. Schematic (top view) of a unit cell of a hexagonally packed pore array, at the maximum pore size ($r = a/2$).

new oxide layer grows up from the bottom.[32] Then, the pore structures in the hexagonal array will eventually merge with each other and have slender pillar-like structures emerging out of the junction area. If the anodization process evolves further, the high-aspect-ratio tip structures will bundle together and form nanocarpet-like structures.[33−35] Figure 1a−f illustrates such progress and varying structural morphologies with the increasing anodization duration, including what we call in this study, planar pore (PP), pore-widened PP, single pillar-on-pore (S-POP), S-POP of high-aspect-ratio sharpened tips, bundled pillar-on-pore (B-POP), and B-POP of an increased bundle size, respectively.

3. EXPERIMENTAL SECTION

3.1. Anodization Processes for the Fabrication of Hybrid Nanostructures. For the anodization processes for the fabrication of hybrid nanostructures, high purity (99.9995%) aluminum foils (Goodfellow, 100 mm × 300 mm × 0.5 mm) were first prepared, being degreased in acetone and ethanol by ultrasonication for 10 min, and rinsed in deionized water. Subsequently, each specimen was electropolished in a mixture of perchloric acid and ethanol ($HClO_4$/C_2H_5OH = 1:4 in volumetric ratio) under an applied potential of 20 V for 3 min at 15 °C to remove surface irregularities. The polished specimen was used as a working electrode (anode) in electrochemical anodization processes, and a platinum electrode was employed as a counter electrode (cathode). The two electrodes were separated by a distance of 5 cm. In the anodization experiments, both the hard anodization (HA)[27] and mild anodization (MA) modes[23−26] were tested in an attempt to create pillar-on-pore hybrid nanostructures. In HA mode, the aluminum substrate was anodized in 0.3 M oxalic acid at 1 °C under various anodizing voltages and intervals to determine the optimal anodizing conditions for the hybrid nanostructure patterns. In MA mode, the aluminum substrate was anodized in 0.1 M phosphoric acid at 10 °C and the anodizing voltages and intervals were also varied to determine the proper conditions for the hybrid-type nanostructures. During the anodization processes, the solution was agitated by a magnetic stirrer to help maintain the uniform anodization process over the sample surface.

3.2. Hydrophobic Surface Treatment. For the testing of superhydrophobic efficiency, the fabricated surface samples were coated with a self-assembled monolayer (SAM) of FDTS (1*H*,1*H*,2*H*,2*H*-perfluorodecyltrichlorosilane, Alfa Inc.). Before being coated, the samples were cleaned by O_2 plasma (Harrick plasma) for 15 min in order to remove organic residues and make the surfaces hydrophilic for the effective amphiphilic monolayer coating. To examine the initial surface hydrophilicity, a static contact angle of a sessile droplet (~3 μL) of deionized water was measured on each sample at room conditions. The contact angles measured on planar porous surfaces were 10−25° (less on pore-widened PP surface with a larger pore size), while those on S-POP and B-POP hybrid nanostructured surfaces were close to 0°. The water droplet spread and permeated quickly (less than 1 s) on the S-POP and B-POP

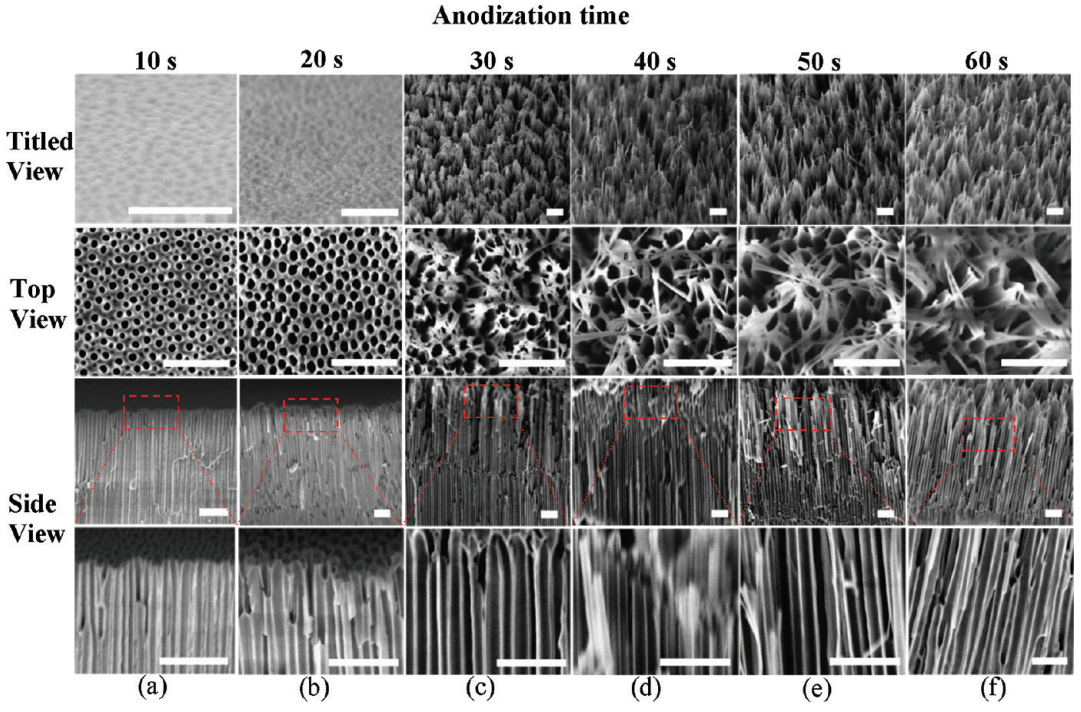

Figure 3. Scanning electron microscope (SEM) images of alumina nanostructures fabricated by a hard anodization (HA) process at 130 V and 1 °C in 0.3 M oxalic acid with varying anodization intervals (0−60 s by every 10 s): (a) PP nanostructures; (b) S-POP nanostructures of low-aspect-ratio tips; (c−f) B-POP nanostructures with increasing bundle sizes. Each row represents titled, top, and side views, respectively. The last row shows higher magnification images of the sidewalls of the base pore structures. Scale bars = 1 μm.

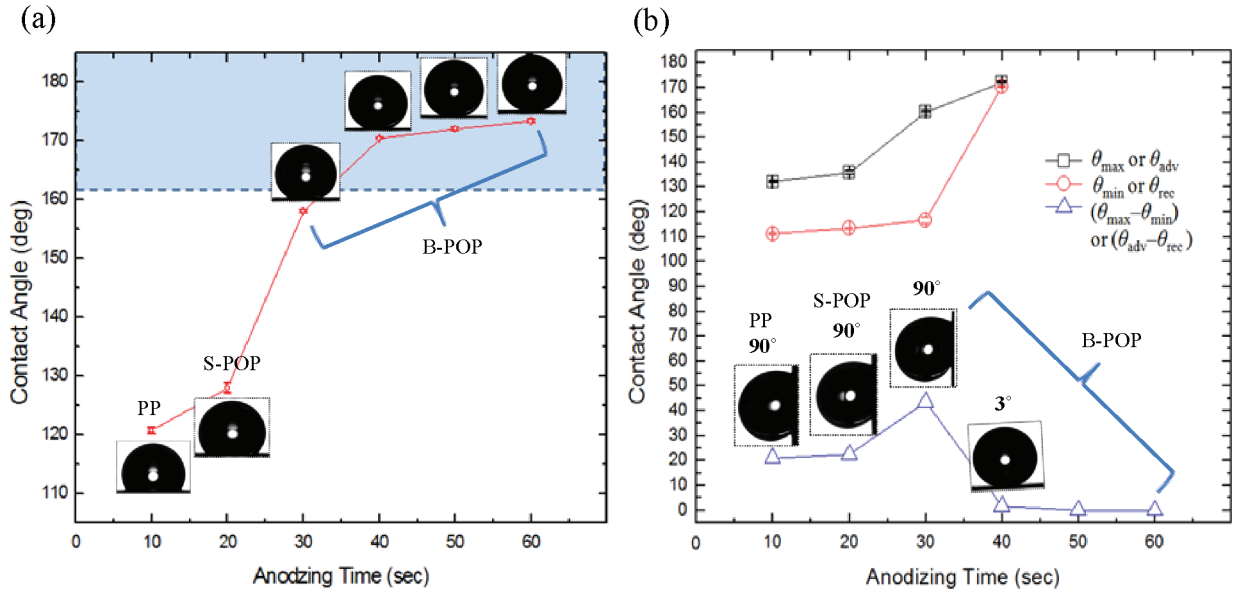

Figure 4. Characterization results of superhydrophobic efficiency of the nanostructured alumina substrates shown in Figure 3, after a hydrophobic monolayer coating. (a) Static contact angles of a water droplet. The contact angles of B-POP structures at 50 and 60 s were measured with the dispensing needle retained in the droplet in order to hold the droplet in place. The dotted line at 162° represents the maximum contact angle theoretically expected on a hexagonal PP array. (b) Dynamic contact angles and hysteresis. In the cases of PP, S-POP, and B-POP at 30 s, a droplet was pinned even at the vertical position. In the completely pinned cases, the maximum and minimum angles measured at the lower and upper contact lines of the droplet (θ_{max} and θ_{min}) were plotted instead of advancing and receding contact angles (θ_{adv} and θ_{rec}), respectively, and their difference ($\theta_{max} - \theta_{min}$) was plotted on behalf of the contact angle hysteresis ($\theta_{adv} - \theta_{rec}$). In the case of B-POP at 40 s, the droplet rolled off at the inclination angle of 3°. In the case of B-POP at 50 and 60 s, the fully dispensed droplet immediately rolled off even at zero inclination so that the measurement of dynamic angles was not available, suggesting little (~0°) contact angle hysteresis.

Table 1. Summary of the Superhydrophobic Efficiency of the Fabricated Samples

anodization mode	structure type (anodization time)	static CA[f] (deg) (ave ± STD)	maximum or advancing CA (deg) (ave ± STD)	minimum or receding CA (deg) (ave ± STD)	CAH[g] (deg)	rolling-off angle (deg)
oxalic acid, HA[a]	PP (10 s)[c]	120.8 ± 0.5	132.2 ± 0.4	111.2 ± 0.3	>21	N/A[h] (pinned)
	S-POP (20 s)[d]	127.9 ± 0.8	135.9 ± 0.8	113.4 ± 0.6	>22.5	N/A (pinned)
	B-POP (30 s)[e]	158.0 ± 0.3	160.2 ± 0.1	116.7 ± 1	>43.5	N/A (pinned)
	B-POP (40 s)	170.5 ± 0.1	172.2 ± 0.2	170.5 ± 0.5	1.7	3
	B-POP (50 s)	172.0 ± 0.3	N/A[h] (rolled off)	N/A (rolled off)	~0	~0
	B-POP (60 s)	173.3 ± 0.3	N/A (rolled off)	N/A (rolled off)	~0	~0
phosphoric acid, MA[b]	S-POP	172.3 ± 0.3	N/A (rolled off)	N/A (rolled off)	~0	~0

[a]HA: hard anodization. [b]MA: mild anodization. [c]PP: planar pore. [d]S-POP: single pillar-on-pore. [e]B-POP: bundled pillar-on-pore. [f]CA: contact angle. [g]CAH: contact angle hysteresis. [h]N/A: not available.

hybrid nanostructured surface, suggesting that the 3D hybrid-type nanostructures make the 2D planar nanostructured surfaces more hydrophilic (i.e., superhydrophilic).[36] Then, hydrophilic samples were coated by the 1 mM FDTS in iso-octane in N_2 drybox at room temperature according to the recipe reported elsewhere,[37] which creates a uniform monolayer film thickness (e.g., ~2 nm). Finally, the samples were rinsed by 2-propanol and water for 5 min and then dried in air for 1 day before the testing of surface superhydrophobicity.

3.3. Characterization of Superhydrophobic Efficiency. For the characterization of the superhydrophobic efficiency of the hydrophobically coated samples, the static and dynamic contact angles of a sessile droplet (~3 μL) of deionized water were measured on each sample at room conditions. A goniometer system (Model 500, Ramehart) was used for the measurements, being capable of automatic tilting of the sample stage for the dynamic measurement. For the measurement of dynamic contact angles (i.e., advancing and receding contact angles at slipping) of the water droplet and the contact angle hysteresis (their difference), the sample stage was gradually tilted from 0 to 90° at the rate of 1° per second and the dynamic contact angles were measured at the moment when a droplet rolled off from the sample's surface. The average and standard deviation values of the contact angles and contact angle hysteresis were obtained by more than three measurements conducted at different locations of each specimen. If the droplet was pinned and did not roll off even at a vertical position (i.e., tilted by 90°), the maximum contact angle (at the lower contact line) and the minimum contact angle (at the upper contact line) were measured on behalf of the advancing and receding contact angles,[38] respectively. In the case of complete pinning, the contact angle hysteresis was not determinate but expected to be greater than the differential between the maximum and minimum angles.

4. RESULTS AND DISCUSSION

In the HA mode experiments, it was found that POP hybrid nanostructures were most effectively obtainable at 130 V. Figure 3 shows the fabrication results for different anodizing intervals at the determined conditions. As proposed in Figure 1, the POP hybrid nanostructures of controlled pillar tip morphology including S-POP (Figure 3b) and B-POP (Figure 3c–f) were achieved directly in the HA process at the regulated

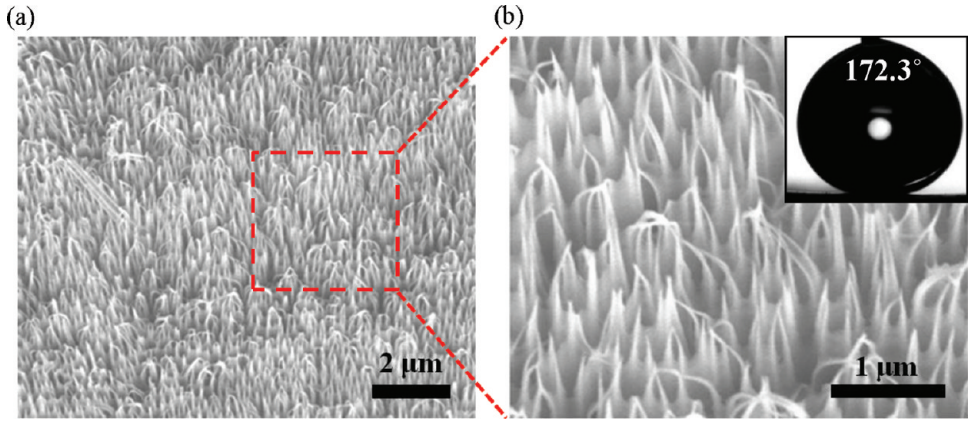

Figure 5. (a) SEM image of high-aspect-ratio single pillar-on-pore (S-POP) nanostructures fabricated by a mild anodization (MA) process at 120 V and 10 °C in 0.1 M phosphoric acid for 20 min. (b) A higher magnification SEM image of (a). The inset in (b) shows a static contact angle (172.3 ± 0.3°) of a water droplet measured on the surface after a hydrophobic monolayer coating. When measuring the contact angle, the dispensing needle tip needed to remain on the top of a droplet to prevent the droplet from immediately rolling off from the surface.

voltage, only by modulating the anodization time. The results demonstrate that POP hybrid-type nanostructures can be conveniently designed and fabricated in the undisrupted single-step anodization process by controlling the anodization parameters. Figure 4 shows the characterization results of the fabricated POP nanostructured surfaces for superhydrophobic efficiency after hydrophobic monolayer coating. The results are also summarized in Table 1.

Figure 4a first displays the static contact angle values of a sessile droplet of water. The results show that the static contact angle increases as the surface evolves from PP (~121°) to S-POP (~128°) to B-POP (up to ~173°). According to the Cassie–Baxter model,[39,40] the apparent contact angle (θ) of a sessile droplet on a composite interface of solid and gas can be described by

$$\cos\theta = r_f \cdot f_{SL} \cos\theta_0 - 1 + f_{SL} \quad (1)$$

where θ_0 is Young's contact angle on a nonpatterned reference surface and f_{SL} is the fraction of a solid–liquid wet surface. r_f is the roughness of the wetted solid surface, which is typically unity for a chemically homogeneous flat-top surface. Equation 1 suggests that a smaller value of f_{SL} will result in a greater contact angle on a superhydrophobic surface. For the case of simple PP patterns, the f_{SL} of the uniform hexagonal pore array illustrated in Figure 2 is reduced to

$$f_{SL} = 1 - \frac{2\pi}{\sqrt{3}} \frac{r^2}{a^2} \quad (2)$$

where r is a pore radius and a is an interpore distance. At the maximum pore size ($r = a/2$), the minimum f_{SL} approaches ~0.1 (~10%). Then, the maximum contact angle expected from the hexagonal PP array is ~162°, which is marked as a dotted line in Figure 4a. While the low-aspect-ratio S-POP (Figure 3b) and B-POP (Figure 3c) nanostructures show the contact angles lower than the theoretical maximum of the PP nanostructures, the contact angles on the high-aspect-ratio B-POP nanostructures (Figure 3d–f) surpass the theoretical limit. This result demonstrates that the POP hybrid nanostructures featured with high-aspect-ratio pillar-like sharp-tip structures can lower the wetted solid-area fraction much below what is attainable by ordinary PP patterns and consequently enhance the surface superhydrophobicity significantly.

Figure 4b further shows the dynamic contact angles (advancing and receding contact angles, θ_{adv} and θ_{rec}, respectively) and their hysteresis (difference between them, i.e., $\theta_{adv} - \theta_{rec}$).[38] On the PP nanostructures (Figure 3a) as well as the low-aspect-ratio S-POP (Figure 3b) and B-POP (Figure 3c) nanostructures, the droplets were strongly pinned on the surface and did not roll off even when tilted to the vertical position. In these cases, the maximum contact angle at the lower contact line (θ_{max}) and the minimum contact angle at the upper contact line (θ_{min}) were used on behalf of the advancing and receding contact angles, respectively. The difference between the maximum and minimum contact angles (i.e., $\theta_{max} - \theta_{min}$) was also used on behalf of the contact angle hysteresis for the plot in Figure 4b. In such a completely pinned case, the advancing contact angle would be greater than the maximum angle while the receding contact angle would be less than the minimum angle[38] so that the actual contact angle hysteresis would be greater than their difference ($\theta_{max} - \theta_{min}$). The result suggests that the low-aspect-ratio S-POP and B-POP nanostructures were not capable of supporting the droplets by only the tip (i.e., top of the pillar structures)[41] so that the droplet intruded and wetted the voids between them, causing the significant pinning.[15] Such pinning effects then increased the contact angle hysteresis and adhesion because of the increased surface contact area and the van der Waals force, as well as capillary pressure.[16,42] Although the exact values of the dynamic contact angles and contact angle hysteresis were not available in the pinned cases, it is still obvious that the contact angle hysteresis on the high-aspect-ratio B-POP nanostructures (Figure 3d–f) were significantly lower (~0°) than those of the PP (>21°) and the low-aspect-ratio S-POP (>22.5°) and B-POP (>43.5°) nanostructures. The remarkably low inclination angle (~0°) at roll-off measured on the high-aspect-ratio B-POP nanostructures further supports the significant reduction of contact angle hysteresis. This clearly shows that the hybridized porous nanostructures with high-aspect-ratio sharpened pillar-like structures, engineered in the proposed anodization process, significantly improve the superhydrophobic efficiency not only in static but also in dynamic conditions.

Meanwhile, it should be noted that S-POP nanostructures with a high-aspect-ratio pillar morphology (similar to that illustrated in Figure 1d) were not conveniently attainable at the tested HA condition (e.g., the sequential anodizing progress

Table 2. Comparison of Superhydrophobic Efficiency of Porous Alumina Nanostructures

references	anodizing condition (additional treatment)	hydrophobic coating	pattern type	contact angle	contact angle hysteresis
C. Ran (2008)[43]	phosphoric acid (etching: 5 wt % phosphoric)	none	PP	132.2°	no data
D. Brevnov (2004)[44]	0.4 M phosphoric acid, 25 °C, 80 V	FC[a]	PP	150°	no data
M. Kemell (2006)[45]	0.3 M sulfuric acid, 10 °C, 25 V (etching: 10 wt % phosphoric acid)	8 × ODS[b]	PP	153°	30°
D. H. Kim (2011)[46]	0.3 M oxalic acid, 10 °C, 45 V (etching: 5 wt % phosphoric acid)	PPFC[c]	B-POP	154°	5.7°
H. Wang (2008)[47]	0.5 M phosphoric acid, 10−20 °C	TODS[d]	PP	157.8°	no data
W. Lee (2009)[32]	0.3 M oxalic acid, 15 °C, 40 V (etching: 5 wt % phosphoric acid)	HDFS[e]	S-POP	166.6°	9°
this work	0.1 M phosphoric acid, 10 °C, 120 V	FDTS[f]	S-POP	172.3°	∼0°
this work	0.3 M oxalic acid, 1 °C, 130 V	FDTS	B-POP	173.4°	∼0°

[a]FC: fluoro carbon. [b]ODS: *n*-octa-decyltrimethoxy-silane. [c]PPFC: plasma polymerized fluoro carbon. [d]TODS: trichloro-octa-decyl-silane. [e]HDFS: hepta-deca-fluoro-1,1,2,2-tetrahydrodecyl-trichloro-silane. [f]FDTS: 1*H*,1*H*,2*H*,2*H*-perfluoro-decyl-trichloros-silane.

every 10 s). It was due to the high etch rate characteristic of the HA process that it was not efficient to regulate the anodization time and realize the S-POP of high-aspect-ratio tips effectively. In contrast, a mild anodization (MA) mode, having a much slower etch rate characteristic, was efficient to achieve better regularity of the pillar nanostructures morphology and produce the high-aspect-ratio S-POP nanostructures. In the tested MA mode, the hybrid-type nanostructures were most effectively obtained at 120 V, including the S-POP nanostructures of high-aspect-ratio tips. For example, Figure 5 shows the high-aspect-ratio S-POP nanostructures achieved in the MA mode. The high-aspect-ratio pillar structures of the S-POP nanostructures were not bundled but mostly retained the single tip structures. After a hydrophobic coating, the high-aspect-ratio S-POP nanostructures were measured to have a static contact angle of 172.3 ± 0.3° with almost zero contact angle hysteresis (see also Table 1), demonstrating excellent superhydrophobic efficiency, similar to the high-aspect-ratio B-POP nanostructures. This result verifies that S-POP and B-POP nanostructures of controlled aspect ratios of the pillar-like tip structures can effectively be designed and created by regulating the anodization processes not only in HA but also in MA mode.

As summarized in Table 2 for comparison, several studies have reported the application of porous alumina nanostructures to superhydrophobic surfaces.[32,43−47] However, most structures realized in those studies were ordinary PP types. Although a few have observed the feasibility of forming pillar-like structures on top of the porous layer in anodization processes, hence the S-POP/B-POP-type nanostructures, the anodizing parameters were not systematically studied and modulated so that they had very limited aspect ratios of the pillar-like top structures. Thus, their contact angles could not exceed the theoretical limit of the simple PP surface, and their contact angle hystereses were also relatively large. In contrast, the hybrid nanoporous structures demonstrated in this study, such as the B-POP and S-POP engineered to have high-aspect-ratio pillars on the top, indeed show the superior superhydrophobic efficiency of a larger contact angle and a lower contact angle hysteresis, which are essential for various applications of superhydrophobic surfaces in both static and dynamic conditions. Furthermore, the fabrication processes adopted by others were relatively complicated, requiring additional surface treatment such as a separate etching step after the initial anodization process.[32,46] In contrast, our results demonstrate that the S-POP and B-POP of high-aspect-ratio pillar nanostructures are directly attainable in a simple one-step anodization process only by regulating the anodizing voltage and time in both HA and MA modes.

Due to great manufacturability, anodizing processes have been commonly and widely used in industries for surface treatment (e.g., oxidation and dyeing) of metallic parts and substrates including aluminum alloys, titanium, zinc, magnesium, niobium, and tantalum, even for ferrous metals such as iron or carbon steel metal. In addition to aluminum material, electrochemical anodization processes have been used to create porous nanostructures of such various metallic materials.[48,49] Therefore, our results further suggest that well-controlled anodization processes can open a new way for creating efficient hybrid-type superhydrophobic surfaces of various metallic substrates in a convenient and effective way similar to that for aluminum as demonstrated in this study. Without any hydrophobic surface treatment, the pillar-on-pore hybrid nanostructures of metal oxides make the surface more hydrophilic (i.e., superhydrophilic). In addition to the superhydrophobic applications demonstrated in this study, such superhydrophilic surfaces also have many potential applications in surface and interfacial transport phenomena such as separation membranes, adsorption, and heat transfer.[36,50] Thus, the pillar-on-pore hybrid nanostructures that can tune the surface wettability of metallic materials effectively via simple anodizing processes will beneficially broaden the applicability of superhydrophobic and -hydrophilic surfaces with enhanced efficacy and nanomanufacturability.

5. CONCLUSIONS

In this paper, we have successfully demonstrated pillar-on-pore hybrid-type nanostructured surfaces with regulated aspect ratios of the top pillar structures by developing a simple one-step anodization process engineered for aluminum substrates. The initial pillar-on-pore hybrid nanostructures of metal oxides created by anodization significantly enhanced the surface hydrophilicity, making them superhydrophilic. Then, after a monolayer hydrophobic coating, the novel hybrid-type porous nanostructures reinforced with high-aspect-ratio sharp-tip pillar-like nanostructures on the top exhibited superior superhydrophobic efficiency with a high contact angle (>173°) and a low contact angle hysteresis (∼0°), overcoming the theoretical limit of the maximum contact angle attainable on a conventional planar hexagonal porous surface (∼162°). The hybrid-type pillar-on-pore nanostructures possess the advantages of both pillar and pore arrays for superhydrophobicity such that the pillar-like tip structures are disconnected so as to allow a high contact angle with a low hysteresis, while the bottom porous surface isolates the retained air layer through the cell walls so as to enhance the dewetting stability. Such

hybrid-type nanostructures with enhanced surface superhydrophobicity will be of great benefit for many engineering systems requiring sustainable and robust superhydrophobic efficiency and dewetting stability for multifunctional applications such as hydrodynamic drag reduction, anticorrosion, antibiofouling, and anti-icing. The enhanced superhydrophilicity of the pillar-on-pore hybrid nanostructures of metal oxides, with no hydrophobic surface treatment applied, will also be useful for many applications associated with surface and interfacial phenomena of materials. The simple and efficient electrochemical anodization technique demonstrated in this study has great potential for the design and fabrication of efficient hybrid-type superhydrophobic and −hydrophilic surfaces on various metallic substrates. Its low cost and scalability makes the anodization technique readily transferrable to manufacturing industries and material processing for immediate impact.

AUTHOR INFORMATION

Corresponding Author

*Phone: 201-216-5579. Fax: 201-216-8315. E-mail: cchoi@stevens.edu.

ACKNOWLEDGMENTS

This work was supported by the Office of Naval Research (ONR) under the Young Investigator Program (YIP). The authors would like to thank Dr. Perez Airan at the ONR and Dr. Keith Sheppard at Stevens Institute of Technology for motivating the idea investigated in this work and for providing insights about the results.

REFERENCES

(1) Onda, T.; Shibuichi, S.; Satoh, N.; Tsujii, K. *Langmuir* **1996**, *12*, 2125−2127.
(2) Nakajima, A.; Hashimoto, K.; Watanabe, T. *Monatsh. Chem.* **2001**, *132*, 31−41.
(3) Feng, X.; Jiang, L. *Adv. Mater.* **2006**, *18*, 3063−3078.
(4) Blossey, R. *Nat. Mater.* **2003**, *2*, 301−306.
(5) Choi, C.-H.; Kim, C.-J. *Phys. Rev. Lett.* **2006**, *96*, 066001.
(6) Choi, C.-H.; Ulmanella, U.; Kim, J.; Ho, C.-M.; Kim, C.-J. *Phys. Fluids* **2006**, *18*, 087105.
(7) Zhang, F.; Zhao, L.; Chen, H.; Xu, S.; Evans, D. G.; Duan, X. *Angew. Chem., Int. Ed.* **2008**, *47*, 2466−2469.
(8) Cao, L.; Jones, A. K.; Sikka, V. K.; Wu, J.; Gao, D. *Langmuir* **2009**, *25*, 12444−12448.
(9) Sarshar, M. A.; Swarctz., C.; Hunter., S.; Simpson., J.; Choi., C.-H. In *Proceedings of ASME IMECE*, Denver, Colorado, November 11−17, 2011, IMECE2011-63282.
(10) Xu, W.; Leeladhar, R.; Tsai, Y.-T.; Yang, E.-H.; Choi, C.-H. *Appl. Phys. Lett.* **2011**, *98*, 073101.
(11) Choi, C.-H.; Kim, C.-J. *Nanotechnology* **2006**, *17*, 5326−5333.
(12) Li, X.-M.; Reinhoudt, D.; Crego-Calama, M. *Chem. Soc. Rev.* **2007**, *36*, 1350−1368.
(13) Roach, P.; Shirtcliffe, N. J.; Newton, M. I. *Soft Matter* **2008**, *4*, 224−240.
(14) Ma, M.; Hill, R. M. *Curr. Opin. Colloid Interface Sci.* **2006**, *11*, 193.
(15) Öner, D.; McCarthy, T. J. *Langmuir* **2000**, *16*, 7777−7782.
(16) Yoshimitsu, Z.; Nakajima, A.; Watanabe, T.; Hashimoto, K. *Langmuir* **2002**, *18*, 5818−5822.
(17) Lee, C.; Kim, C.-J. *Phys. Rev. Lett.* **2011**, *106*, 014502.
(18) Bahadur, V.; Garimella, S. V. *Langmuir* **2009**, *25*, 4815−4820.
(19) Jessensky, O.; Muller, F.; Gosele, U. *Appl. Phys. Lett.* **1998**, *72*, 1173−1175.
(20) Li, F.; Zhang, L.; Metzger, R. M. *Chem. Mater.* **1998**, *10*, 2470−2480.
(21) Chu, S. Z.; Wada, K.; Inoue, S.; Isogai, M.; Yasumori, A. *Adv. Mater.* **2005**, *17*, 2115−2119.
(22) Houser, J. E.; Hebert, K. R. *Nat. Mater.* **2009**, *8*, 415−420.
(23) Masuda, H.; Fukuda, K. *Science* **1995**, *268*, 1466−1468.
(24) Masuda, H.; Hasegwa, F.; Ono, S. *J. Electrochem. Soc.* **1997**, *144*, L127−L130.
(25) Masuda, H.; Yada, K.; Osaka, A. *Jpn. J. Appl. Phys., Part 2* **1998**, *37*, L1340−L1342.
(26) Li, A. P.; Muller, F.; Birner, A.; Nielsch, K.; Gosele, U. *J. Appl. Phys.* **1998**, *84*, 6023−6026.
(27) Lee, W.; Ji, R.; Gosele, U.; Nielsch, K. *Nat. Mater.* **2006**, *5*, 741−747.
(28) Ono, S.; Saito, M.; Asoh, H. *Electrochem. Solid-State Lett.* **2004**, *7*, B21.
(29) Lee, W.; Nielsch, K.; Gosele, U. *Nanotechnology* **2007**, *18*, 475713.
(30) Zhang, R.; Jiang, K.; Ding, G. *Thin Solid Films* **2010**, *518*, 3797−3800.
(31) Yang, C.; Tartaglino, U.; Persson, B. N. J. *Phys. Rev. Lett.* **2006**, *97*, 116103.
(32) Lee, W.; Park, B. G.; Kim, D. H.; Ahn, D. J.; Park, Y.; Lee, S. H.; Lee, K. B. *Langmuir* **2009**, *26*, 1412−1415.
(33) Lau, K.; Bico, J.; Teo, K.; Chhowalla, M.; Amaratunga, G.; Milne, W.; McKinley, G.; Gleason, K. *Nano Lett.* **2003**, *3*, 1701−1705.
(34) Fan, J.-G.; Dyer, D.; Zhang, G.; Zhao, Y.-P. *Nano Lett.* **2004**, *4*, 2133−2138.
(35) Zhao, Y.-P.; Fan, J.-G. *Appl. Phys. Lett.* **2006**, *88*, 103123.
(36) Drelich, J.; Chibowski, E.; Meng, D. D.; Terpilowski, K. *Soft Matter* **2011**, *7*, 9804−9828.
(37) Srinivasan, U.; Houston, M. R.; Howe, R. T.; Maboudian, R. *J. Microelectromech. Syst.* **1998**, *7*, 252−259.
(38) Krasovitski, B.; Marmur, A. *Langmuir* **2005**, *21*, 3881−3885.
(39) Cassie, A. B. D.; Baxter, S. *Trans. Faraday Soc.* **1944**, *40*, 546−551.
(40) Barbieri, L.; Wagner, E.; Hoffmann, P. *Langmuir* **2007**, *23*, 1723−1734.
(41) Choi, C.-H.; Kim, C.-J. *Langmuir* **2009**, *25*, 7561−7567.
(42) Lai, Y.; Gao, X.; Zhuang, H.; Huang, J.; Lin, C.; Jiang, L. *Adv. Mater.* **2009**, *21*, 3799.
(43) Ran, C.; Ding, G.; Liu, W.; Deng, Y.; Hou, W. *Langmuir* **2008**, *24*, 9952−9955.
(44) Brevnov, D. A.; Barela, M. J.; Brooks, M. J.; Lopez, G. P.; Atanassov, P. B. *J. Electrochem. Soc.* **2004**, *151*, B484.
(45) Kemell, M.; Farm, E.; Leskela, M.; Ritala, M. *Phys. Status Solidi A* **2006**, *203*, 1453−1458.
(46) Kim, D. H.; Kim, Y.; Kim, B. M.; Ko, J. S.; Cho, C. R.; Kim, J. M. *J. Micromech. Microeng.* **2011**, *21*, 045003.
(47) Wang, H.; Dai, D.; Wu, X. *Appl. Surf. Sci.* **2008**, *254*, 5599−5601.
(48) Ruan, C.; Paulose, M.; Varghese, O. K.; Mor, G. K.; Grimes, C. A. *J. Phys. Chem. B* **2005**, *109*, 15754−15759.
(49) Wu, X.; Bai, H.; Zhang, J.; Chen, F. e.; Shi, G. *J. Phys. Chem. B* **2005**, *109*, 22836−22842.
(50) Bocquet, L.; Lauga, E. *Nat. Mater.* **2011**, *10*, 334−337.